Int J Appl Earth Obs Geoinformation 78 (2019) 138–148

Contents lists available at ScienceDirect

Int J Appl Earth Obs Geoinformation

journal homepage: www.elsevier.com/locate/jag

The potential of retrieving snow line dynamics from Landsat during the end of the ablation seasons between 1982 and 2017 in European mountains

Zhongyang Hu*, Andreas Dietz, Claudia Kuenzer

German Remote Sensing Data Center (DFD), Earth Observation Center (EOC), German Aerospace Center (DLR), Oberpfaffenhofen, Wessling, Germany

ARTICLE INFO

Keywords:
Landsat
Snow
Europe
Mountains
Snow line elevation
Time-series

ABSTRACT

Snow cover in the Northern Hemisphere is continuously decreasing during the ablation seasons in the context of climate change. Snow Line Elevation (SLE) is a suitable indicator illustrating detailed snow cover distribution dynamics at a regional scale. In order to carry out time-series analyses of the SLEs in mountain areas, long-term (> 30 years) and detailed spatial resolution (< 100 m) data are required. In this article, we have retrieved SLEs from Landsat during the end of the ablation seasons in European mountains between 1984 and 2017. Based on our analyses, it is possible to use the Landsat archive to illustrate potential long-term snow line dynamics in the Alps, the Carpathian Mountains, and the Pyrenees. The snow lines appear to recede to higher elevations in these Southern European Mountains. To further implement statistical analyses, it is required to fill the missing observations, and reduce uncertainties induced by intermediate snowfall events.

1. Introduction

Snow is the most widely distributed cryospheric component during winter, covering up to 45.2 million km^2 of the land surface in the Northern Hemisphere (Lemke et al., 2007). Snow cover dynamics are of great importance regarding freshwater availability, hydropower generation, biodiversity, radiation budget, tourism, and natural hazards (e.g., snowmelt-induced floods or avalanches). Additionally, snow has been identified as an Essential Climate Variable (ECV) by the Global Climate Observing System (GCOS) (Mason et al., 2003), which is hence an essential measure for the ongoing climate change. In response, the European Space Agency (ESA) introduced the Climate Change Initiative (CCI) program to better support the observations of snow and other ECVs. Severity and impact of climate change vary significantly among regions. Mountains embody fragile ecosystems (Beniston et al., 1997; Diaz et al., 2003), whilst providing various ecosystem services and socio-economic wellbeing. In Europe, mountains cover approximately 2 million km^2 and are inhabited by more than 94 million people (Schuler et al., 2004). The majority of the annual runoff in European montane catchments is snowmelt-dominated (Barnett et al., 2005). The European Union (EU) White Paper on adaptation to climate change (EC, 2009) identified the mountain areas as one of the most climate-sensitive and vulnerable regions in Europe, and significant responses have been observed and projected in mid-latitude mountains in the context of climate change (IPCC, 2014 2013). The European Environment Agency (EEA) assessed the high vulnerability of the Alps, the “water towers of Europe”, with respect to decreasing summer runoff induced by the diminishing snow and glacier cover (EEA, 2009). Together with a subsequent report on climate change across the entire Europe (EEA, 2017), EEA emphasized the necessity of enhanced observations and research to bridge knowledge gaps pertaining to climate change adaptation. In this view, observing snow cover dynamics in mountain areas would not only expand our comprehension of the regional responses to ongoing climate change, but also support the decision-making and development of evidence-based adaptation strategies.

Satellite-based Earth Observation (EO) has a long history of monitoring snow which leads back to the 1960s, when the National Oceanic and Atmospheric Administration/National Environmental Satellite, Data, and Information Service (NOAA/NESDIS) started to provide weekly binary snow cover charts of the Northern Hemisphere based on the Environmental Science Services Administration-3 (ESSA-3) satellite data (Matson and Wiesnet, 1981). Today, EO data still plays a crucial role in snow observation, including mapping Snow Cover Area (SCA), characterizing snow parameters (e.g., snow depth, snow grain size, snow water equivalent and snow impurity), and monitoring snowmelt processes (Hu et al., 2017). Among these, SCA is one of the most frequently derived parameters. To derive SCA, optical EO data are frequently being employed due to the readily, fast, accurate and robust methods (Hall et al., 1995; Klein et al., 1998; Riggs et al., 1994). Snow cover distribution during the ablation season is essential with regards to

* Corresponding author.
E-mail address: zhongyang.hu@dlr.de (Z. Hu).

https://doi.org/10.1016/j.jag.2019.01.010
Received 20 July 2018; Received in revised form 7 November 2018; Accepted 16 January 2019
Available online 12 February 2019

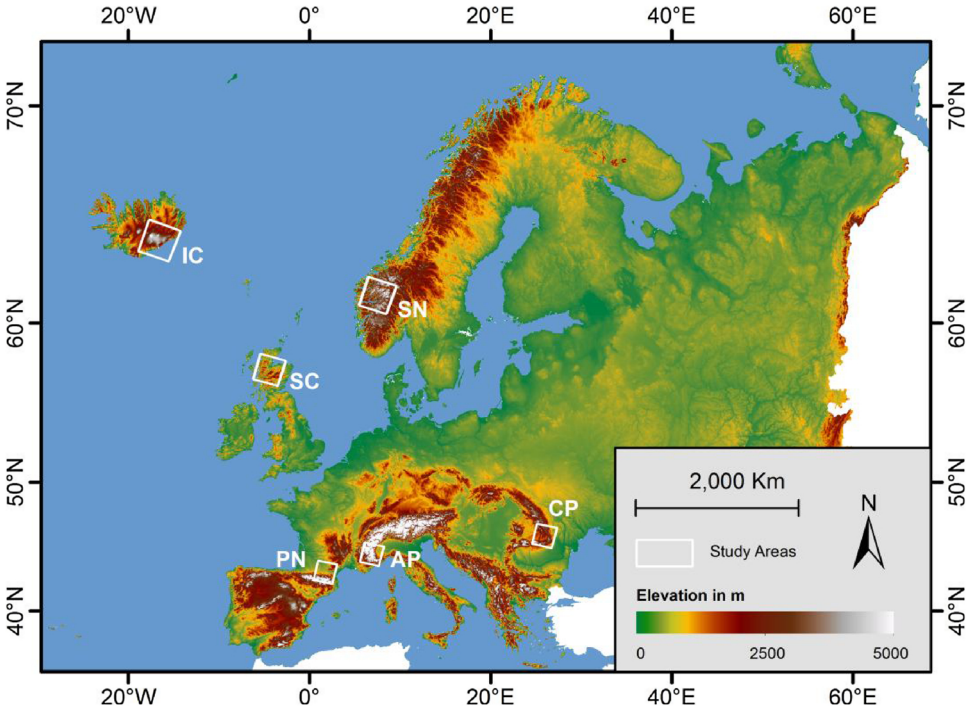

Fig. 1. Digital Elevation Model (DEM) and selected study areas/sites in the Scandinavian Mountains (SN, Landsat Footprint Path/Row: 200/017), Scotland (SC, Landsat Footprint Path/Row: 206/020), Iceland (IC, Landsat Footprint Path/Row: 217/015), the Pyrenees (PN, Landsat Footprint Path/Row: 198/030), the Alps (AP, Landsat Footprint Path/Row: 195/029) and the Carpathian Mountains (CP, Landsat Footprint Path/Row: 183/028).

runoff generation, winter sports/tourism, and ongoing climate change. There is a high confidence that SCA during the ablation season in the Northern Hemisphere is continuously decreasing (IPCC, 2013). To further assess the detailed mountainous snow cover distribution dynamics at a regional scale, Snow Line Elevation (SLE) is a suitable indicator (Krajčí et al., 2014; Parajka et al., 2018). SLEs can be derived based on SCAs and a Digital Elevation Model (DEM). Monitoring the transition zone between the snow-covered and snow-free area in mountain regions for an extended time-series could reveal possible effects of climate change on snow cover distribution. However, retrieving snow cover distribution under the complex terrain, based on prevalently employed medium to coarse spatial resolution data (e.g., Moderate Resolution Imaging Spectroradiometer (MODIS), Advanced Very High Resolution Radiometer (AVHRR)), could be error-prone (Blöschl, 1999; Painter et al., 2009; Severskiy and Zichu, 2000). Therefore, a spatial resolution of 100 m or better is recommended in mountain areas (GCOS, 2016). Moreover, to assess the snow dynamics in the context of climate change, the World Meteorological Organization (WMO) suggested a monitoring period of at least 30-year (WMO, 2007). Landsat, providing 30 m spatial resolution and long-term (i.e. over four decades) data records, would therefore be particularly intriguing for long-term snow cover distribution assessment in mountain areas.

At present, Landsat is the longest uninterrupted operating EO program which also offers free access since 2008 (Wulder et al., 2012). Landsat-based snow studies have been conducted since the 1970s (Barnes and Bowley, 1973), and snow-related EO topics are being investigated by the current (2018–2023) Landsat Science Team. In May 2018, the United States Geological Survey (USGS) unprecedentedly reorganized the global Landsat 1–5 Multispectral Scanner (MSS), Landsat 7 Enhanced Thematic Mapper Plus (ETM+), Landsat 8 Operational Land Imager/Thermal Infrared Sensor (OLI/TIRS), and the majority of Landsat 4–5 Thematic Mapper (TM) scenes into the USGS Collection 1 archive. After this reorganization, time-series analyses based on Landsat have become much more feasible owing to the consistent generation of geometrically- and radiometrically-calibrated and tiered products (USGS/EROS, 2017). Yet only a limited number of Landsat-based snow studies (e.g. Crawford et al., 2013; Macander et al., 2015; Sankey et al., 2015; Wayand et al., 2018) were carried out at a time-series level of more than 30 years. To our knowledge, there is no existing study that examines snow cover dynamics in European mountains based on long-term Landsat time-series. This lack of Landsat-based long-term snow cover studies in European mountains might be caused by three distinct reasons: data gaps caused by technical and managerial problems, near-two-week revisit time, and cloud cover.

The objective of this study is to assess the potential of the Landsat archive for retrieving long-term Snow Line Elevation (SLE) dynamics during the end of the ablation seasons in European mountains. The following aspects have been analyzed for this purpose: (1) the availability of cloud-free Landsat observations across Europe, in particular the mountain areas; (2) the opportunities and challenges of retrieving SLEs during the end of the ablation seasons based on the Landsat archive. Given the signal saturation of Landsat 1–5 MSS data over snow and ice (Altena and Kääb, 2017) and the absence of the thermal band, Landsat 1–5 MSS data have been excluded from this study. For long-term time-series analyses in cloud-prone areas, for example snow-covered mountain areas (Martinuzzi et al., 2007; USGS/EROS, 2017), USGS suggests lowering the selection criterion from Tier 1 (i.e. “stackable” data for time-series analysis) to Level 1 Precision and Terrain (L1TP) processing level to filter out unsuitable time-series input scenes (USGS/EROS, 2017).

2. Study areas and data

2.1. Study areas

For the purpose of assessing mountainous snow cover dynamics in Europe, six study areas distributed across Europe are selected. These areas include regions of the Scandinavian Mountains (SN), Scotland (SC), Iceland (IC), the Pyrenees (PN), the Alps (AP), and the Carpathian Mountains (CP). To examine the potential of Landsat data for analyzing the time-series of SLEs, one footprint in each study area is selected (Fig. 1). The footprint selection criteria include: 1) high Landsat data availability, 2) low overall cloud cover frequency, and 3) a distinct gradient of topography ranging from lower lying plains to high-elevated mountains. Therefore, the results presented are from footprints that benefit from near-optimal Landsat data availability and low cloud cover frequency.

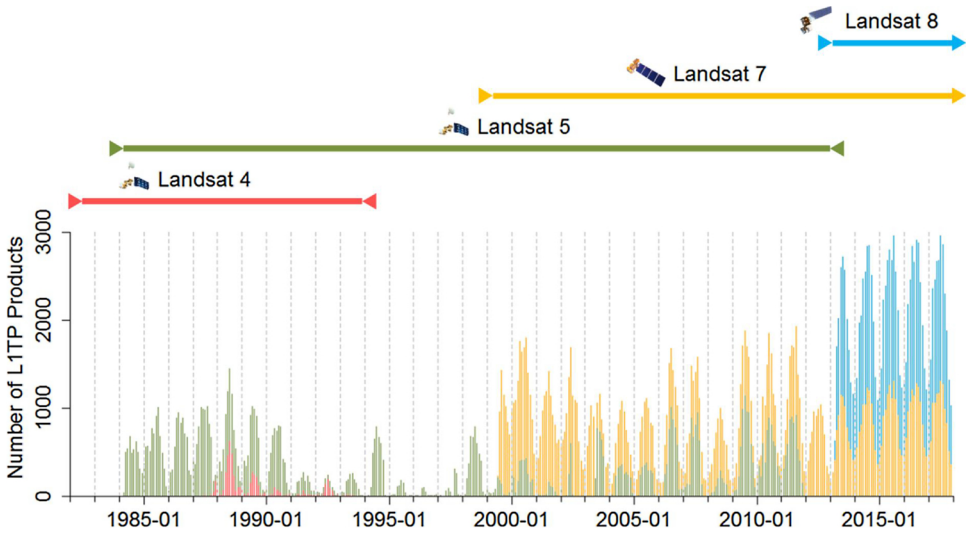

Fig. 2. Temporal pattern of monthly Landsat 4–5 TM, Landsat 7 ETM + and Landsat 8 OLI/TIRS L1TP acquisitions over Europe archived in the USGS Landsat Collection 1 dataset between 1982 and 2017.

2.2. Landsat data

To obtain an overview of the Landsat data availability in USGS Landsat Collection 1 archive (USGS/EROS, 2017) between 1982 and 2017 across Europe, the archive's metadata collection (January 16, 2018) has been analyzed. Fig. 2 summarizes the temporal pattern of monthly Landsat availability with the peak appearing in summer and the minimum in midwinter. Also, two data gaps (1982–1984 and 1991–1999) have been identified. Hypothetically, some ascending scenes (i.e. "night-time" acquisitions) might provide additional usable observations during the polar day in Northern Europe. But according to the examined metadata, more than 93% of the ascending scenes contain sun elevations below 15°, which are therefore not appropriate for accurate atmospheric correction and post-processing. Hence, to systematically detect snow cover and cloud cover, only the descending USGS Landsat Surface Reflectance Level-2 Science Products processed at L1TP level are utilized in this study. They encompass the Landsat Ecosystem Disturbance Adaptive Processing System (LEDAPS) products for Landsat TM and ETM + scenes, and the Landsat 8 Surface Reflectance Code (LaSRC) products for Landsat 8 OLI/TIRS scenes.

2.3. Auxiliary data

For the purpose of validation, the snow classification results are evaluated by daily snow depth observations from the European Climate Assessment & Dataset (ECA&D). Within the selected study areas, the ECA&D data are originating from 45 meteorological stations at different elevations ranging from 4 to 2519 m between 1984 and 2017. To determine the SLEs, the Advanced Spaceborne Thermal Emission and Reflection Radiometer (ASTER) Global Digital Elevation Model Version 2 (GDEM V2) (Tachikawa et al., 2011) are employed. Moreover, Global SnowPack (GSP, a MODIS-based daily SCA product, Dietz et al., 2015) and contemporary Sentinel-2 (S-2) nearly-cloud-free (< 20% cloud cover) scenes are adopted to evaluate and validate the final SLE results. The GSP is based on the daily MODIS snow cover product MOD10A1 (Riggs and Hall, 2015) and consists of daily, cloud-free information about the global snow cover extent at 500 m resolution. Fig. 3 illustrates the Snow Depletion Curves (SDCs) in cyanic color as derived from the GSP within mountain areas (elevation > 600 m) for each study area. The SDCs indicate the remaining mean snow cover area (in percentage) during the end of the ablation seasons between 2000 and 2017. The red/blue bars indicate the mean SCA changes compared with the previous day. A red bar (negative value) of the point indicates that snow is melting. Vice versa, a blue bar (positive value) means that snow is accumulating, i.e. there is a fresh snowfall event. Since GSP is a daily SCA product, it is possible to estimate the glaciated and firn-covered areas by identifying the pixels covered by snow/ice for no less than 90% of the days from 2000 to 2017. Firn and glacier ice are then colored in dark blue in the SDCs. S-2 nearly cloud-free scenes (within ± 3 days) are used to validate the SLE results in the corresponding Landsat cloud-covered pixels. In terms of the S-2 scenes preparation, the Carpathian Mountains and Iceland are excluded due to missing cloud-sparse S-2 observations and insufficient Landsat SLE results, respectively.

3. Methods

3.1. Snow cover classification and validation

To classify snow cover, two pre-processing steps are implemented to avoid misclassifications in bright and warm, or dark surfaces, using the thresholds introduced by the ESA Satellite Snow Product Intercomparison and Evaluation Exercise (SnowPEX) Team (Ripper et al., 2015). Firstly a thermal threshold (< 288 K) is set to filter out bright and warm surfaces (e.g., warm rocks). Subsequently, cast-shadowed areas and dark surfaces are excluded by thresholding the visible band at 0.55 µm (reflectance < 0.2), the mid infrared band at 1.6 µm (reflectance < 0.02), and the Normalized Difference Vegetation Index (NDVI < 0.1). Followed by these pre-processing steps, the snow-covered areas are determined by applying thresholds on the Normalized Difference Snow Index (NDSI) and NDVI, which was proposed by Klein et al. (1998) and complemented by several modifications introduced by Metsämäki et al. (2015) and Poon and Valeo (2006). The results are validated using the contemporary ECA&D snow depth observations, with a 1 cm snow depth threshold following Parajka et al. (2010b).

3.2. Cloud detection

For cloud screening, the Level-2 "Pixel Quality Assurance Bit Band" (i.e. "pixel_qa") provided by both LEDAPS and LaSRC products are used, which is simplified by the indication of cloud confidence, cloud shadow and snow/ice flags based on the C Function of Mask (CFMask) algorithm (Foga et al., 2017; Zhu and Woodcock, 2012; Zhu et al., 2015). CFMask is a multi-pass algorithm that uses decision trees to prospectively label pixels in the scene; it then validates or discards those labels according to scene-wide statistics. It also creates a cloud shadow mask by iteratively estimating cloud heights and projecting

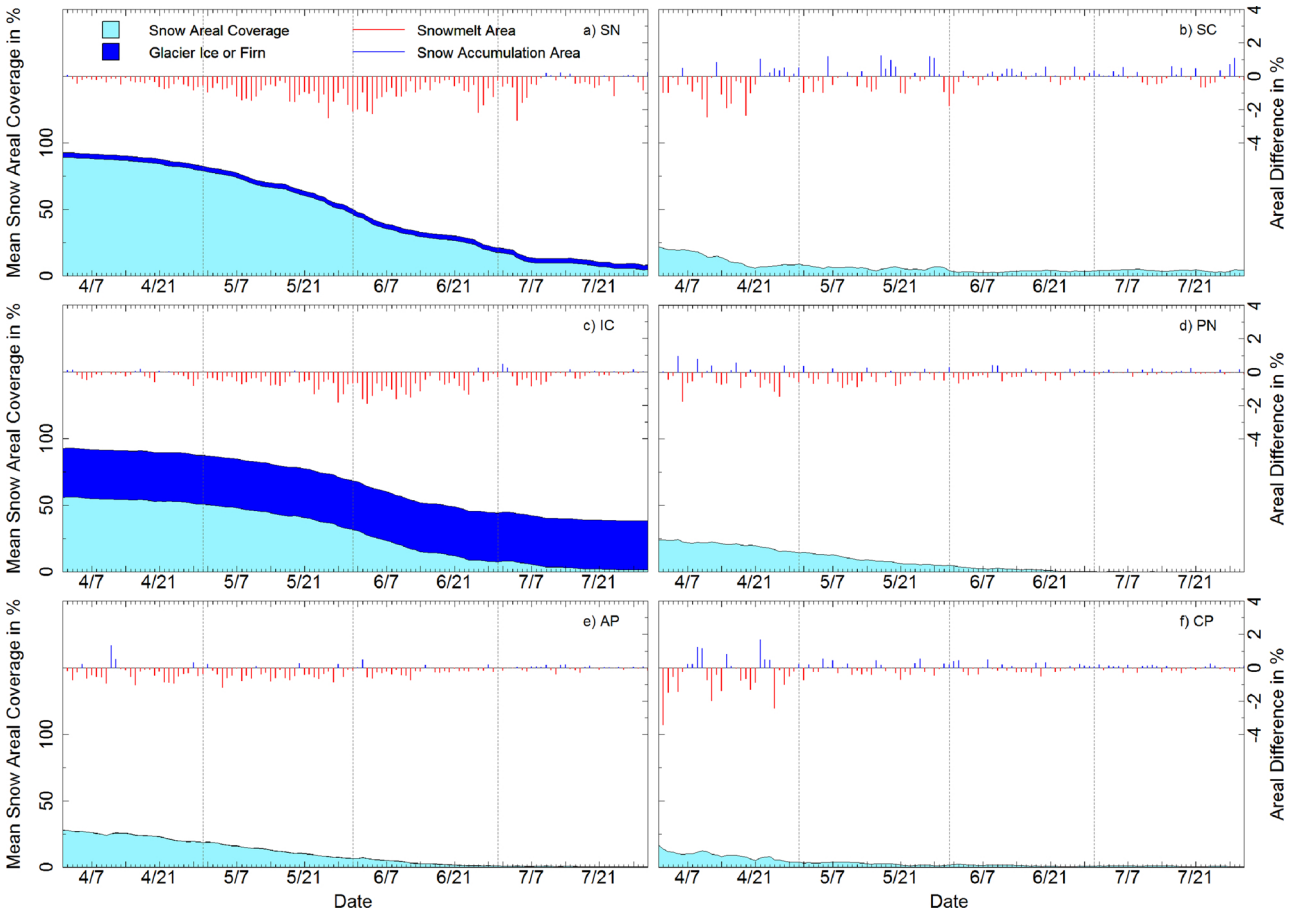

Fig. 3. MODIS-derived Snow Depletion Curves (SDCs) and mean snow areal coverage difference compared to the previous day (red/blue bars)between 2000 and 2017 for the selected study areas at Landsat footprint extent: a) the Scandinavian Mountains (SN, Path/Row: 200/017), b) Scotland (SC, Path/Row: 206/020), c) Iceland (IC, Path/Row: 217/015), d) the Pyrenees (PN, Path/Row: 198/030), e) the Alps (AP, Path/Row: 195/029) and f) the Carpathian Mountains (CP, Path/Row: 183/028) (For interpretation of the references to colour in this figure legend, the reader is referred to the web version of this article).

them onto the ground. The accuracy of CFMask has been widely examined by e.g., Foga et al. (2017); Qiu et al. (2017), and Selkowitz and Forster (2015). The cloud mask is hereafter applied to the obtained SCA results to create the final snow classification map.

3.3. Snow line elevation retrieval and accuracy assessment

To derive SLEs, the snow lines are delineated for each selected Landsat scene by identifying the border between snow-covered and snow-free areas. SLEs are subsequently extracted from the DEM by tracking the identified snow lines for each Landsat scene on a pixel basis. To capture the snow line dynamics at the end of the ablation seasons, the statistics (including 10%, 25%, 75% and 90% percentile; median and mean) are calculated and displayed in whisker-boxplots year-wise for April (the Carpathian Mountains and Scotland), May (the Alps, Pyrenees), June (Iceland) and July (the Scandinavian Mountains) between 1984 and 2017. The abovementioned months are selected to guarantee: 1) infrequently occurrence of snowfall events; 2) relatively equivalent (approximately 20%) snow coverage among the study areas; 3) Minimized effect of glaciated and firn-covered areas; 4) frequent availability of cloudless Landsat acquisitions for each study area. For demonstration, median SLEs at the end of the ablation seasons are chosen. Given that the derived median SLEs are only statistical measures, the elevation difference of overestimated (snow-free areas above median SLE) and underestimated (snow-covered areas below the median SLE) areas is calculated to assess the representability and spatial accuracy of the derived SLEs. Besides, as the snow classification maps and the employed DEM are both validated or proven accurate, the remaining uncertainty in the SLEs originates from snow lines below clouds. To validate the mean SLE results below clouds, we select higher-resolution nearly-cloud-free (cloud cover < 20%) S-2 images (acquired within ± 3 days of the corresponding Landsat scene). Snow cover in the S-2 scenes is classified based on the same algorithm already described in Section 3.1. Due to the absence of a thermal band, the additional thermal threshold which was used to filter out bright-warm surfaces cannot be applied. Possible misclassifications are manually corrected. Finally, the area above the SLE within the Landsat scene is compared with the S-2 classification result. 200 random points above 600 m are generated for each footprint where the S-2 contains cloud-free data while Landsat is affected by cloud cover. Subsequently, the overall accuracy (OA) is calculated, which is defined as the sum of correctly identified snow pixels divided by the total number of sampled points in percentage:

$$Overall\ Acuracy\ (OA) = (A + D)/(A + B + C + D) \times 100\ [\%] \quad (1)$$

where A, B, C and D represent the number of correctly (A: S-2 snow and above SLE, and C: S-2 snow-free and under SLE) or erroneously (B: S-2 snow and under SLE, and D: S-2 snow-free and above SLE) classified points in a particular category after SLEs are retrieved.

4. Results

4.1. Long-term availability of Landsat obervations for snow line elevation retrieval

In mountain areas, approximately 500 acquisitions per footprint are

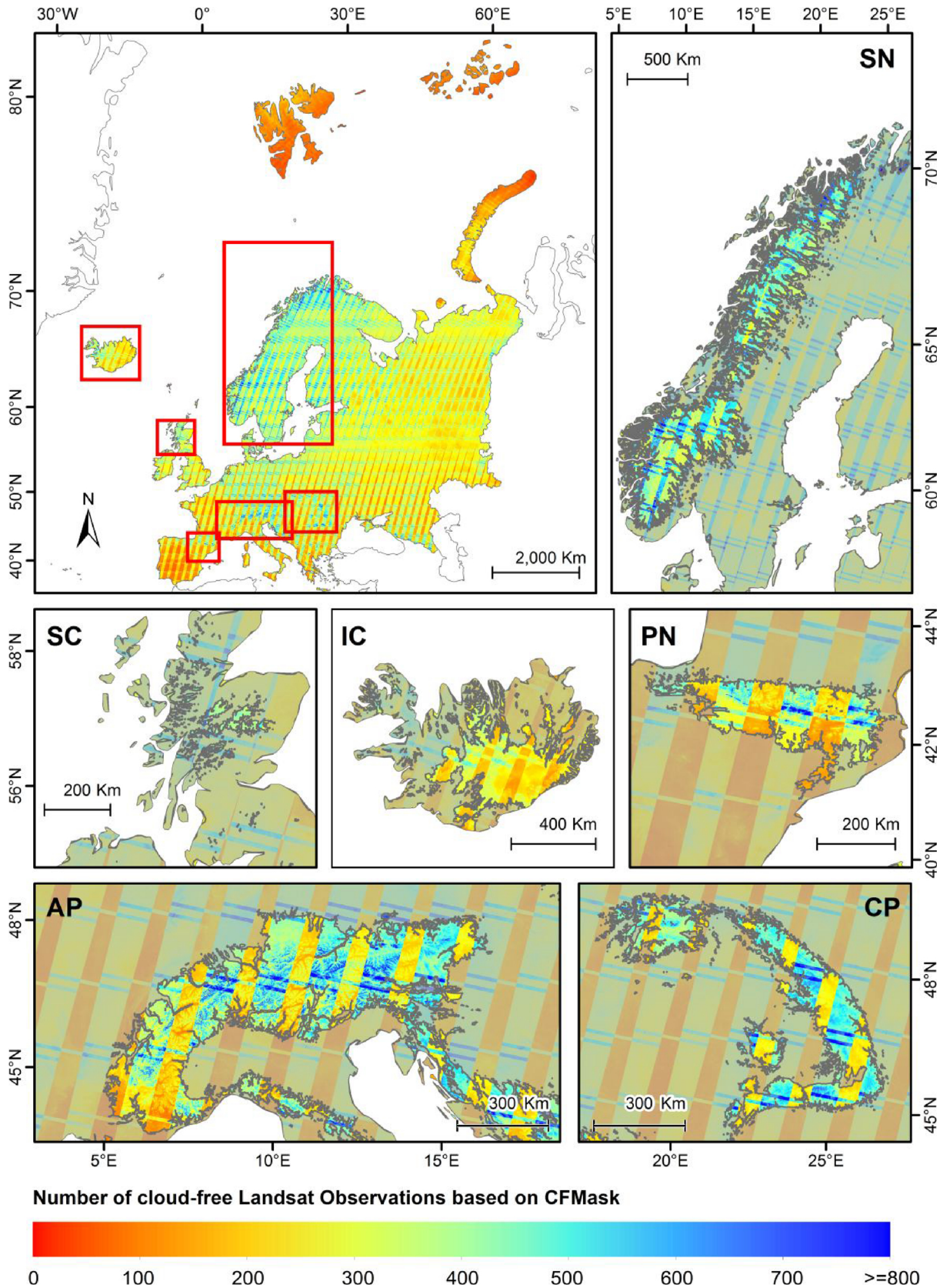

Fig. 4. Spatial distribution of Landsat 4–5TM, Landsat 7 ETM + and Landsat 8 OLI/TIRS L1TP pixel-based cloud-free observations over Europe archived in Collection 1 dataset between 1984 and 2017.

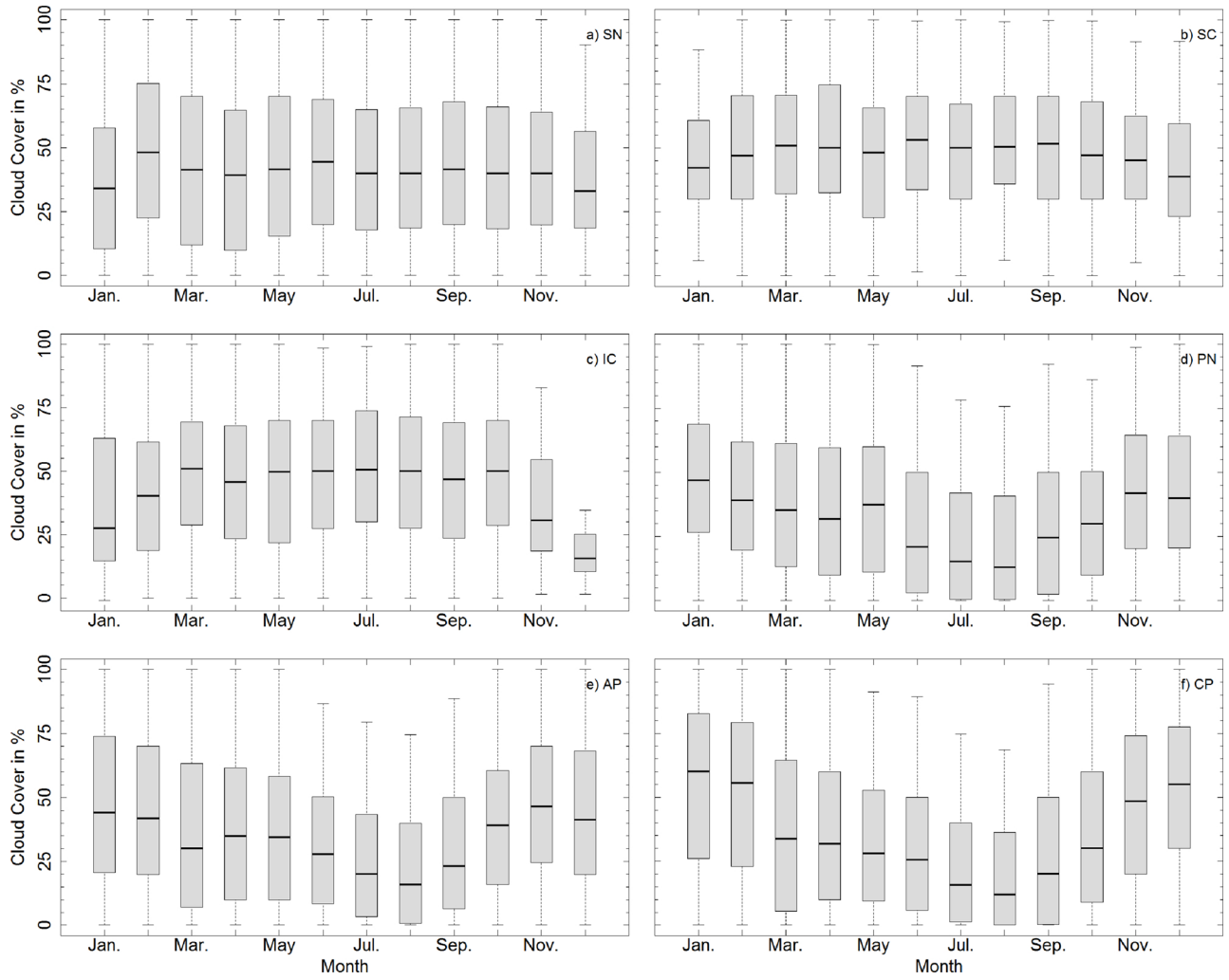

Fig. 5. Box-whisker plots representing 10%, 25%, 50%, 75% and 90% percentiles of scene-wise seasonal cloud cover percentage in the selected mountain areas: a) the Scandinavian Mountains (SN), b) Scotland (SC), c) Iceland (IC), d) the Pyrenees (PN), e) the Alps (AP), and f) the Carpathian Mountains (CP).

archived in Collection 1 over the Alps, and a similar number of images are also acquired over the Carpathian Mountains and the Pyrenees. The mountains in Northern Europe have deficient acquisitions, especially those located on islands (e.g., Iceland and Scotland). For optical snow monitoring, clouds do not only obstruct optical EO observation, but also cause challenges in separating snow and clouds. Mountain areas tend to be more frequently (> 70% of the time) cloud-covered. Taking the cloud cover frequency into consideration, the Alps, the Carpathian Mountains and the Pyrenees still have the highest quantities of Landsat cloud-free acquisitions (see Fig. 4). The number of available scenes can reach more than 1000 at locations where footprints overlap (e.g., in the Northern Alps and the Central Carpathians). These effects are particularly pronounced in Europe.

The seasonal cloud cover patterns from the selected six mountain areas are illustrated in Fig. 5. They are calculated based on the cloud flags in the Landsat metadata files scene-wise. The Scandinavian Mountains (Fig. 5a), Scotland (Fig. 5b) and Iceland (Fig. 5c) are the most cloud-prone areas among all months, where the median cloud coverage accounts for around 40% throughout the whole year. The upper quantiles of the cloud cover in these areas persist at approximately 70% in each month. In addition, the clouds are much more persistent in Scotland and Iceland, whose lower quantiles of cloud cover are generally above 30% and 20%, respectively. A detected anomaly is the cloud cover over Iceland in December (Fig. 5c), which is obviously lower than in other months. The intra-annual cloud cover variations of mountains in Southern Europe (the Alps, the Carpathian Mountains, and the Pyrenees) present a cosine-curve shape. Most of the Landsat summer acquisitions have less than 50% cloud coverage. The lower quantiles stay approximately at 5% in July and August.

4.2. Snow line dynamics during the end of the ablation seasons

To demonstrate the snow cover fluctuations during the end of the ablation seasons, the statistics of SLEs during the end of the ablation seasons are displayed in whisker-boxplots (Fig. 6) for each study area between 1984 and 2017. The SLEs are generally lower in high-latitude areas (i.e. the Scandinavian Mountains, Scotland and Iceland) than in low-latitude areas during the end of the ablation seasons. It is challenging to explicitly delineate the snow lines, since: 1) high-latitude areas are in lack of Landsat L1TP products, in particular in Iceland and Scotland, there are only 19 and 17 years in which Iceland and Scotland has Landsat observations at L1TP level during the selected month; 2) apart from the Scandinavian Mountains and Iceland, the cloud cover fractions around the snow line often (> 50% of the time) account for more than 50% in some years, particularly in the Carpathian Mountains. Intermediate snowfall events in the Alps and the Pyrenees are visible as comparably variable boxplots of long interquartile range and/or overall low SLEs. In general, the snow lines appear to recede to higher elevations in Southern European Mountains since 1984 (i.e., the Alps, and the Pyrenees).

Fig. 6. Box-whisker plots representing 10%, 25%, 50%, 75% and 90% percentiles of Snow Line Elevations (SLEs) and the mean SLEs (blue dots) during the end of the ablation-season between 1984 and 2017 in the selected study areas: a) the Scandinavian Mountains (SN, Path/Row: 200/017) during July, b) Scotland (SC, Path/Row: 206/020) during April, c) Iceland (IC, Path/Row: 217/015) during June, d) the Pyrenees (PN, Path/Row: 198/030) during May, e) the Alps (AP, Path/Row: 195/029) during May and f) the Carpathian Mountains (CP, Path/Row: 183/028) during April (For interpretation of the references to colour in this figure legend, the reader is referred to the web version of this article).

To further visualize the spatial dynamics of the SLEs, the frequencies of snow-covered areas during the end of the ablation seasons based on the median SLEs are displayed in Fig. 7 for the Scandinavian Mountains, Scotland, the Alps, the Pyrenees, and the Carpathian Mountains. Higher fluctuations of SLEs are visible in the Southern European Mountains when compared to the Scandinavian Mountains, which is consistent with a possible snow line retreat in these areas as illustrated in Fig. 6. In Southern European Mountains, there are large areas characterized by less frequent snow coverage, which correspond with the occurrence of the overall low SLEs in Fig. 6.

4.3. Accuracy assessment

The spatial accuracy assessment of the overestimated (snow-free areas above median SLE) and underestimated (snow-covered areas below the median SLE) areas is illustrated in Fig. 8. In general, overestimation mostly occurs in the southern slope of the Southern European mountains, while underestimation is mostly observed on the northern slope thereof. Underestimation is also frequently observed in glaciers and ice caps periphery areas, such as Jostedal Glacier (Norway). It is also discovered that spatial patterns of the erroneous areas coincide with areas of more prone to precipitation because of their location on windward slopes. The region with the largest over- and underestimation is the Vatnajökull ice cap (Iceland). On the windward slope near the coastline, large underestimated areas are observed and displayed in Fig. 8. The same pattern is also observed in Scotland.

There are three main sources of the derived SLE uncertainties: 1) misclassifications in the SCA maps, 2) errors of the DEM employed, and 3) uncertainties of the cloud-covered areas in the SCA maps. Since the accuracy of ASTER GDEM has been studied by other researchers (e.g., Hirt et al., 2010; Reuter et al., 2009; Tachikawa et al., 2011) and would stay as a systematic error for SLE change detection, we assess only the two remaining error sources. The accuracy of the SCA maps has been reported as 96.43%, according to 1222 ECA&D observations based on 1 cm snow depth criterion. Table 1 summarizes the validation of SLE results based on higher resolution S-2 images regarding the uncertainties in the Landsat cloud-covered areas. In general, the retrieved SLEs achieve an overall accuracy of around 80.50%, with higher uncertainties discovered in glaciated areas (particularly in the Scandinavian Mountains and Iceland). Details regarding producer's and user's accuracies can be found in Table 1.

5. Discussion

5.1. Discontinuity in Landsat archive over Europe

In the previous sections, Landsat data gaps, as well as the uneven

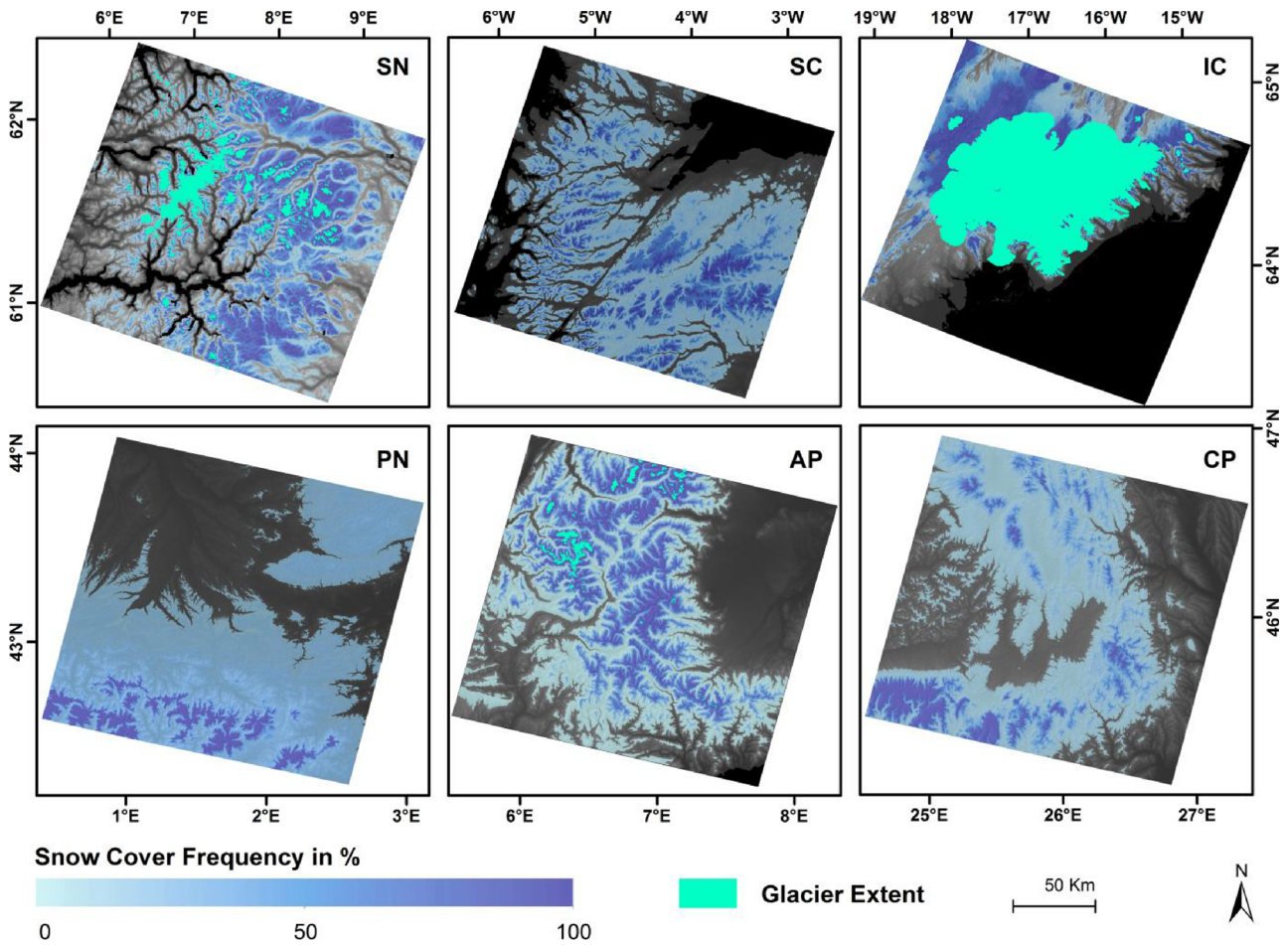

Fig. 7. Snow cover frequencies during the end the of the ablation seasons based on Landsat-derived median Snow Line Elevations (SLEs) between 1984 and 2017 in the selected mountain areas: a) the Scandinavian Mountains (SN, Path/Row: 200/017) during July, b) Scotland (SC, Path/Row: 206/020) during April, c) the Pyrenees (PN, Path/Row: 198/030) during June, d) the Alps (AP, Path/Row: 195/029) during May and e) the Carpathian Mountains (CP, Path/Row: 183/028) during April. The base-map is a hill-shade derived from the Digital Elevation Model (DEM). Cyan color represents glaciers based on the Randolph Glacier Inventory (RGI).

spatiotemporal distribution of Landsat Collection 1 datasets in Europe, have been addressed. These data gaps and the heterogeneous distribution are mainly triggered by four reasons: (1) satellite technical failures (mainly the transmitter failures, e.g., Chander et al., 2007; Chander and Micijevic, 2006), (2) commercialization attempts (also known as "the era of privatization", see Goward et al., 2006), (3) data sharing and shortage, and (4) the acquisition priority plans. Missing observations due to technical failures and commercialization attempts can hardly be overcome. Alternative satellite data (e.g., the French satellite 'Satellite Pour l'Observation de la Terre' (SPOT) Constellation) could potentially provide an opportunity to fill the gaps in this period. The impacts of data sharing and shortage are critical, as reported by Goward et al. (2006). The total number of Landsat data stored in the International Cooperators' (ICs) archives far exceeds those in the USGS archive, and large quantities of these data are unique and not duplicated in the USGS Landsat archive (Wulder et al., 2016). Among the ICs, ESA holds most historical Landsat MSS/TM/ETM+/OLI/TIRS images (> 1.5 million) (Goward et al., 2006; Saunier et al., 2017). In Europe, ~ 500,000 Landsat 5TM images archived at ESA's KIS station could not be geometrically and radiometrically corrected due to the missing Payload Correction Data (PCD) files (Micijevic et al., 2017; Wulder et al., 2016). Once these images could be processed, the Landsat availability in Europe might be improved considerably. Regarding the preferential acquisition plan, i.e., the Long Term Acquisition Plan (LTAP, details see Arvidson et al., 2006, 2001), it would potentially cause a deficit of data availability in high-altitude and (especially) high-latitude areas due to the impacts of low sun elevations and severe cloud cover. Furthermore, influences such as the Landsat 7 ETM + Scan Line Corrector (SLC) failure (Markham et al., 2004) and some anomalies and artifacts recognized by USGS (https://landsat.usgs.gov/known-issues) should also be noted with regards to the Landsat data availability and utility.

Cloud cover is one of the most interfering factors concerning optical EO data availability and methodological feasibility. In terms of snow line retrieval, cloud coverage of less than 70%~90% has been suggested as a premise by Gafurov and Bárdossy (2009); Krajčí et al. (2014); Parajka et al. (2010a), to name a few. Since the cloud information is derived from the CFMask-based cloud flag, the accuracy of SLE results is also significantly affected by the performance of the cloud detection algorithm (i.e., CFMask). Although the overall accuracy of CFMask was reported as 96.4% by Zhu and Woodcock (2012), commission errors of the CFMask over bright targets such as ice/snow, sand dunes, rocks and building roofs have been well-recognized by the remote sensing community (e.g., reported in Selkowitz and Forster, 2015). Moreover, the cloud flags in USGS LEDAPS and LaSRC products are generated using the default 22.5% cloud probability and three-pixel buffer. This three-pixel buffer amplifies the commission errors of the CFMask. In this context, it is strongly recommended to refine and revise the cloud mask when mapping snow/ice-covered areas. Apart from the cloud mask, we realize that the implemented snow classification method is actually insensitive to thin haze. The method has successfully detected a large quantity of snow/ice under thin haze and cloud shadows while excluding the existing clouds. Therefore, further studies are needed to

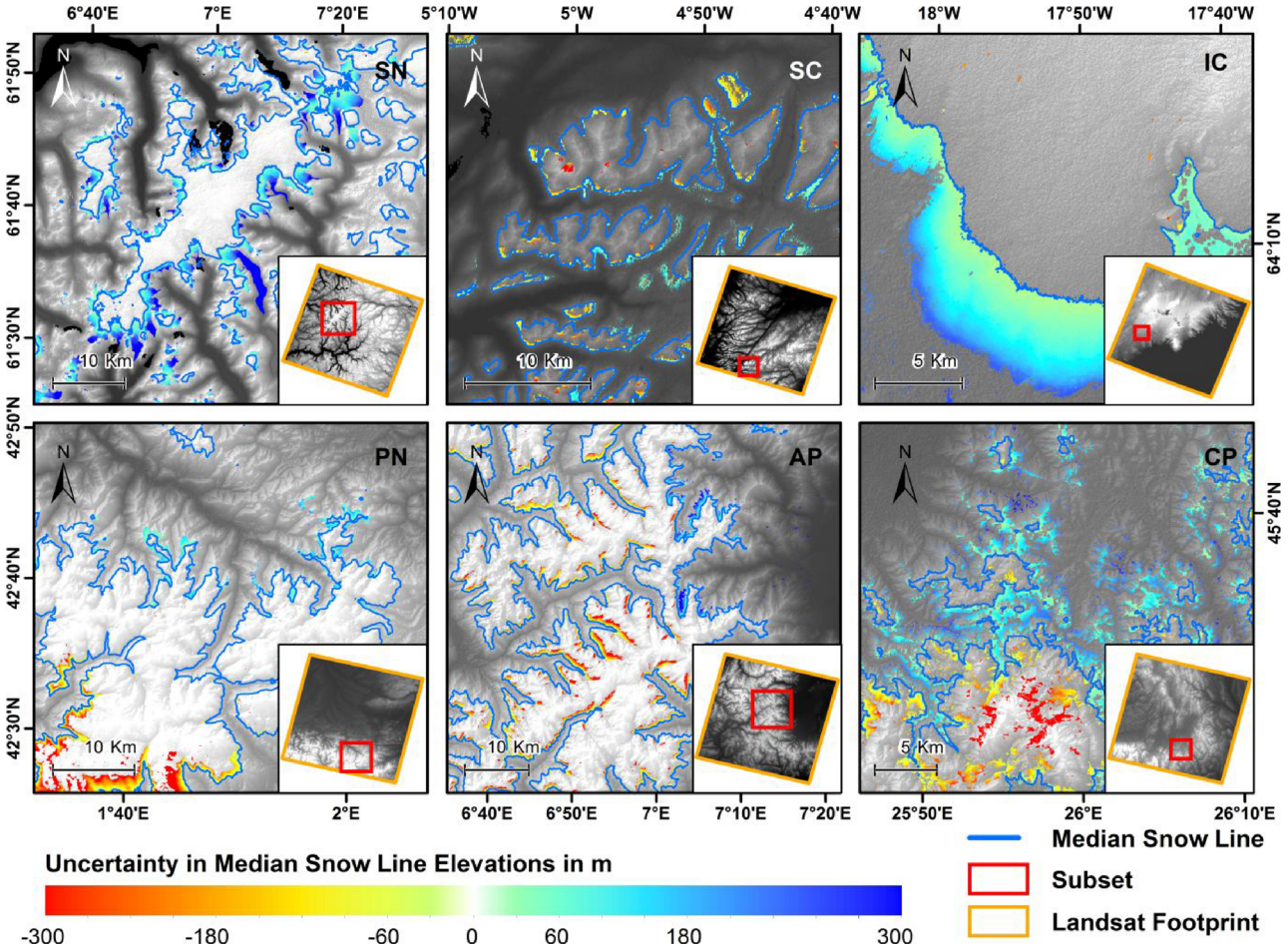

Fig. 8. Details of the spatial uncertainty assessment of the median Snow Line Elevations (SLEs) during the end of the ablation seasons between 1984 and 2017 for the selected mountain areas: a) the Scandinavian Mountains (SN, Path/Row: 200/017) during July, b) Scotland (SC, Path/Row: 206/020) during April, c) the Pyrenees (PN, Path/Row: 198/030) during June, d) the Alps (AP, Path/Row: 195/029) during May and e) the Carpathian Mountains (CP, Path/Row: 183/028) during April. Red color indicates overestimated areas (snow-free areas above median SLE) and blue color indicates underestimated areas (snow-covered areas below the median SLE). The base-map is a hill-shade derived from the Digital Elevation Model (DEM) (For interpretation of the references to colour in this figure legend, the reader is referred to the web version of this article).

Table 1
Confusion matrix relating the Sentinel-2 cloud-free binary snow observations and the Landsat-derived mean Snow Line Elevations (SLEs) at the end of the ablation seasons.

	Above Landsat SLE	Under Landsat SLE	User's Accuracy
Sentinel-2 Snow	228	39	85.39%
Sentinel-2 Snow-free	195	738	79.10%
Producer's Accuracy	53.90%	94.98%	OA = 80.50%

investigate the aforementioned cloud and haze influences, especially quantitative analyses of snow/cloud confusion under different cloud coverages and cloud types. It would improve not only the accuracy of SCA results, but also the representativeness of the derived SLEs.

5.2. Opptunities and challenges of Snow Line Elevation (SLE) determination from Landsat

The results shown in Section 4.2 indicate a potential of the long-term time-series analysis of Landsat-derived SLEs in some European mountains (e.g., the Alps, the Carpathian Mountains, and the Pyrenees). A possible tendency of snow line retreat is suggested by the SLE results. To further conduct statistical analyses of the SLE dynamics, more studies are required to address the following challenges/factors:

5.2.1. Determination of the end of the ablation season

Due to possible intermediate snowfall events within the near-two-week revisit time, it is challenging to derive snow distribution dynamics throughout the whole ablation season (Hall and Martinec, 1986). Therefore, the determination of the end of the ablation season provides a good balance among between the frequency of fresh snowfall, persistence of observable snow, exposure of glacier ice, and availability of cloudless scenes. However, following the abovementioned criteria, in fact, intermediate snowfall events could still occur in this month, which weakens the representability of the derived SLEs. Such intermediate snowfall events also create challenges for interpreting the observed SLE anomalies: whether it is induced by climate change or intermediate snowfall. MODIS-derived daily snow cover products (e.g., GSP) could help to interpret these outliers. However, such data are only available after 2000. In this regard, meteorological station records, climate reanalysis data, climate models, and AVHRR data could help to interpret the anomalies.

5.2.2. Missing observations

The missing observations are mainly caused by historical data absence and cloud obstruction. Future studies should focus not only on developing innovative gap-filling technologies for the Landsat archive, but also on incorporating additional EO data to densify the time-series. It is expected that great benefits arise from combining historical

Landsat records with a similarly configured optical sensor such as ASTER, Sentinel-2, China-Brazil Earth Resources Satellite (CBERS), and/or Synthetic Aperture Radar (SAR) sensors (e.g., Environmental Satellite-Advanced Synthetic Aperture Radar (ENVISAT-ASAR), Sentinel-1) to densify the time-series. Moreover, revising the cloud detection would also increase the pixel-based data availability to a large extent.

5.2.3. SLE uncertainties

To more accurately retrieve SLEs, some additional geographical settings should be considered, including topographical aspects, the position relative to the windward/downwind side of a mountain, solar insolation, mountain orientations, and vegetation cover. At a regional scale, glacier-periphery areas tend to have a lower snow line. Given the 16-day revisit time of Landsat, further studies are also essential to deal with the heterogeneous acquisition dates. Noteworthy, the acquisition time also differs for several days amongst the latitudinal adjacent scenes. It is hence not suitable to directly merge these scenes together for studying SLE dynamics, particularly during the accumulation and the end of the ablation seasons due to possible intermediate snowfall events. Some of such events (after year 2000) have been confirmed by the GSP. In this view, Landsat-based snow dynamics studies would benefit from developing a novel method for date homogenization. Also, the benefit from overlapping Landsat footprints should not be neglected, as it could densify the time-series in more than half of the mountain areas.

5.2.4. Validation scheme

Validation of the Landsat-derived SLEs is challenging. The conventional validation scheme using higher resolution optical data is not only economically costly, as these data are often not free-accessible, but there would also still be a high possibility that the areas would still be covered by clouds. Although SAR data are not influenced by cloud cover, accurately classifying dry snow solely using SAR data remains challenging. Alternatively, snow station or snow course data would be an option. On the other hand, obtaining field measurements for a large area could be labor- and material-intensive and challenging in inaccessible mountain areas. Under this condition, Web-Cams offer an alternative potential, as they are comparatively cost-efficient and less influenced by cloud cover.

6. Conclusions

The Landsat archive is a valuable dataset for snow observations, particularly in mountain areas, given its spatial resolution and high radiometric and geometric accuracy. The presented study assesses the potential of retrieving Snow Line Elevations (SLEs) based on Landsat time-series during the end of the ablation seasons in European mountains between 1984 and 2017. The accuracy of the SLEs is assessed using higher resolution Sentinel-2 data and is confirmed to reach 80.50%. According to the results, it is possible to identify potential long-term changes of snow cover distributions during the end of the ablation seasons in some European mountains (e.g., the Alps, the Carpathian Mountains, and the Pyrenees) using Landsat-derived SLEs. Such SLE results would not only facilitate the comprehensions of regional responses to the climate change in climatic-sensitive areas, but also potentially support water resource management, runoff prediction, and winter sports management. In Southern European Mountains, the snow lines appear to recede to higher elevations. However, missing observations, uncertainties induced by intermediate snowfall events, and heterogeneous acquisition dates still need to be addressed soundly, in order to further implement statistical analyses. In the next step, we plan to solve these problems by combining the historical Landsat archive with a similarly configured optical and/or Synthetic Aperture Radar (SAR) data to densify the time-series, and cope with the meteorological station records and climate reanalysis data to interpret and confirm the results.

Acknowledgments

The authors would like to thank the China Scholarship Council for the financial support of this research. The authors would also like to thank the anonymous reviewers for their elaborated and helpful remarks as well as constructive criticism to improve the quality of the paper.

References

Altena, B., Kääb, A., 2017. Elevation change and improved velocity retrieval using orthorectified optical satellite data from different orbits. Remote Sens. 9, 300.
Arvidson, T., Gasch, J., Goward, S.N., 2001. Landsat 7's long-term acquisition plan—an innovative approach to building a global imagery archive. Remote Sens. Environ. 78, 13–26.
Arvidson, T., Goward, S., Gasch, J., Williams, D., 2006. Landsat-7 long-term acquisition plan. Photogramm. Eng. Remote Sens. 72, 1137–1146.
Barnes, J.C., Bowley, C.J., 1973. Use of ERTS data for mapping snow cover in the western United States. Final Rep. under Contract AS5-21803. Environ. Res. Technol. Inc., Concord, MA, pp. 77.
Barnett, T.P., Adam, J.C., Lettenmaier, D.P., 2005. Potential impacts of a warming climate on water availability in snow-dominated regions. Nature 438, 303–309.
Beniston, M., Diaz, H.F., Bradley, R.S., 1997. Climatic change at high elevation sites: an overview. Clim. Change 36, 233–251.
Blöschl, G., 1999. Scaling issues in snow hydrology. Hydrol. Process. 13, 2149–2175.
Chander, G., Micijevic, E., 2006. Absolute Calibration Accuracy of L4 TM and L5 TM Sensor Image Pairs. Earth Observing Systems XI p.62960D.
Chander, G., Helder, D.L., Malla, R., Micijevic, E., Mettler, C.J., 2007. Consistency of L4 TM Absolute Calibration with Respect to the L5 TM Sensor Based on Near-simultaneous Image Acquisition. Earth Observing Systems XII 66770F.
Crawford, C.J., Manson, S.M., Bauer, M.E., Hall, D.K., 2013. Multitemporal snow cover mapping in mountainous terrain for Landsat climate data record development. Remote Sens. Environ. 135, 224–233.
Diaz, H.F., Grosjean, M., Graumlich, L., 2003. Climate variability and change in high elevation regions: past, present and future. Clim. Change 59, 1–4.
Dietz, A.J., Kuenzer, C., Dech, S., 2015. Global SnowPack: a new set of snow cover parameters for studying status and dynamics of the planetary snow cover extent. Remote Sens. Lett. 6, 844–853.
EC, 2009. White Paper-adapting to Climate Change: Towards a European Framework for Action. European Commission (Accessed 19 July 2018). https://ec.europa.eu/health/ph_threats/climate/docs/com_2009_147_en.pdf.
EEA, 2009. Regional Climate Change and Adaptation-The Alps Facing the Challenge of Changing Water Resources. European Environment Agency Copenaghen, Denmark (Accessed 19 July 2018). https://www.eea.europa.eu/publications/alps-climate-change-and-adaptation-2009.
EEA, 2017. Climate Change, Impacts and Vulnerability in Europe 2016 - an Indicator-based Report. Publications Office of the European Union (Accessed 19 July 2018). https://www.eea.europa.eu/publications/climate-change-impacts-and-vulnerability-2016.
Foga, S., Scaramuzza, P.L., Guo, S., Zhu, Z., Dilley, R.D., Beckmann, T., Schmidt, G.L., Dwyer, J.L., Hughes, M.J., Laue, B., 2017. Cloud detection algorithm comparison and validation for operational Landsat data products. Remote Sens. Environ. 194, 379–390.
Gafurov, A., Bárdossy, A., 2009. Cloud removal methodology from MODIS snow cover product. Hydrol. Earth Syst. Sci. 13, 1361.
GCOS, 2016. The Global Observing System for Climate: Implementation Needs (Accessed on 29 May 2018) Available online. https://unfccc.int/sites/default/files/gcos_ip_10oct2016.pdf.
Goward, S., Arvidson, T., Williams, D., Faundeen, J., Irons, J., Franks, S., 2006. Historical record of Landsat global coverage. Photogramm. Eng. Remote Sens. 72, 1155–1169.
Hall, D.K., Martinec, J., 1986. Remote Sensing of Ice and Snow. Chapman and Hall/CRC Press, London.
Hall, D.K., Riggs, G.A., Salomonson, V.V., 1995. Development of methods for mapping global snow cover using moderate resolution imaging spectroradiometer data. Remote Sens. Environ. 54, 127–140.
Hirt, C., Filmer, M.S., Featherstone, W.E., 2010. Comparison and validation of the recent freely available ASTER-GDEM ver1, SRTM ver4. 1 and GEODATA DEM-9S ver3 digital elevation models over Australia. Austrian J. Earth Sci. 57, 337–347.
Hu, Z., Kuenzer, C., Dietz, A.J., Dech, S., 2017. The potential of earth observation for the analysis of cold region land surface dynamics in Europe—a review. Remote Sens. 9, 1067.
IPCC, 2013. Climate Change 2013: the Physical Science Basis: Working Group I Contribution to the Fifth Assessment Report of the Intergovernmental Panel on Climate Change. Cambridge University Press.
IPCC, 2014. Climate Change 2014: Impacts, Adaptation, and Vulnerability-part B: Regional Aspects-contribution of Working Group II to the Fifth Assessment Report of the Intergovernmental Panel on Climate Change. Cambridge University Press.
Klein, A.G., Hall, D.K., Riggs, G.A., et al., 1998. Improving snow cover mapping in forests through the use of a canopy reflectance model. Hydrol. Process. 12, 1723–1744.
Krajčí, P., Holko, L., Perdigão, R.A.P., Parajka, J., 2014. Estimation of regional snowline

elevation (RSLE) from MODIS images for seasonally snow covered mountain basins. J. Hydrol. 519, 1769–1778.
Lemke, P., Ren, J., Alley, R.B., Allison, I., Carrasco, J., Flato, G., Fujii, Y., Kaser, G., Mote, P., Thomas, R.H., et al., 2007. Observations: Changes in Snow, Ice and Frozen Ground. Cambridge University Press.
Macander, M.J., Swingley, C.S., Joly, K., Raynolds, M.K., 2015. Landsat-based snow persistence map for northwest Alaska. Remote Sens. Environ. 163, 23–31.
Markham, B.L., Storey, J.C., Williams, D.L., Irons, J.R., 2004. Landsat sensor performance: history and current status. IEEE Trans. Geosci. Remote Sens. 42, 2691–2694.
Martinuzzi, S., Gould, W.A., González, O.M.R., 2007. Creating Cloud-free Landsat ETM+ Data Sets in Tropical Landscapes: Cloud and Cloud-shadow Removal. US Department of Agriculture, Forest Service, International Institute of Tropical Forestry. Gen. Tech. Rep. IITF-32, pp. 32.
Mason, P.J., Manton, M., Harrison, D.E., Belward, A., Thomas, A.R., Dawson, D.K., 2003. The second report on the adequacy of the global observing systems for climate in support of the UNFCCC. GCOS Rep. 82.
Matson, M., Wiesnet, D.R., 1981. New data base for climate studies. Nature 289, 451–456.
Metsämäki, S., Pulliainen, J., Salminen, M., Luojus, K., Wiesmann, A., Solberg, R., Böttcher, K., Hiltunen, M., Ripper, E., 2015. Introduction to GlobSnow Snow Extent products with considerations for accuracy assessment. Remote Sens. Environ. 156, 96–108.
Micijevic, E., Haque, M.O., Mishra, N., 2017. Radiometric Characterization of Landsat Collection 1 Products. Earth Observing Systems XXII 104021D.
Painter, T.H., Rittger, K., McKenzie, C., Slaughter, P., Davis, R.E., Dozier, J., 2009. Retrieval of subpixel snow covered area, grain size, and albedo from MODIS. Remote Sens. Environ. 113, 868–879.
Parajka, J., Kohnová, S., Bálint, G., Barbuc, M., Borga, M., Claps, P., Cheval, S., Dumitrescu, A., Gaume, E., Hlavčová, K., et al., 2010a. Seasonal characteristics of flood regimes across the Alpine–Carpathian range. J. Hydrol. 394, 78–89.
Parajka, J., Pepe, M., Rampini, A., Rossi, S., Blöschl, G., 2010b. A regional snow-line method for estimating snow cover from MODIS during cloud cover. J. Hydrol. 381, 203–212.
Parajka, J., Bezak, N., Burkhart, J., Hauksson, B., Holko, L., Hundecha, Y., Jenicek, M., Krajčí, P., Mangini, W., Molnar, P., Riboust, P., Rizzi, J., Sensoy, A., Thirel, G., Alberto, V., 2018. MODIS snowline elevation changes during snowmelt runoff events in Europe. J. Hydrol. Hydromech. 67, 101–109. https://doi.org/10.2478/johh-2018-0011.
Poon, S.K.M., Valeo, C., 2006. Investigation of the MODIS snow mapping algorithm during snowmelt in the northern boreal forest of Canada. Can. J. Remote Sens. 32, 254–267.
Qiu, S., He, B., Zhu, Z., Liao, Z., Quan, X., 2017. Improving Fmask cloud and cloud shadow detection in mountainous area for Landsats 4–8 images. Remote Sens. Environ. 199, 107–119.
Reuter, H.I., Neison, A., Strobl, P., Mehl, W., Jarvis, A., 2009. A first assessment of ASTER GDEM tiles for absolute accuracy, relative accuracy and terrain parameters. Geoscience and Remote Sensing Symposium, 2009 IEEE International, IGARSS 2009. pp. V–240.
Riggs, G.A., Hall, D.K., 2015. MODIS Snow Products Collection 6 User Guide. (accessed 19 July 2018). https://modis-snow-ice.gsfc.nasa.gov/uploads/C6_MODIS_Snow_User_Guide.pdf.
Riggs, G.A., Hall, D.K., Salomonson, V.V., 1994. A snow index for the Landsat thematic mapper and moderate resolution imaging spectroradiometer, in: geoscience and remote sensing symposium, 1994. IGARSS'94. Surface and Atmospheric Remote Sensing: Technologies, Data Analysis and Interpretation., International. pp. 1942–1944.
Ripper, E., Bippus, G., Nagler, T., Metsämäki, S., Fernandes, R., Crawford, C.J., Painter, T., Rittger, K., 2015. Guidelines for the Generation of Snow Extent Products from High Resolution Optical Sensors – FINAL. Available online. http://snowpex.enveo.at/Documents/D08_Guidelines_for_the_generation_of_snow_extent_products_from_HR_optical_sensors_FINAL_v1.0.pdf.
Sankey, T., Donald, J., McVay, J., Ashley, M., O'Donnell, F., Lopez, S.M., Springer, A., 2015. Multi-scale analysis of snow dynamics at the southern margin of the North American continental snow distribution. Remote Sens. Environ. 169, 307–319.
Saunier, S., Northrop, A., Lavender, S., Galli, L., Ferrara, R., Mica, S., Biasutti, R., Goryl, P., Gascon, F., Meloni, M., et al., 2017. European Space agency (ESA) Landsat MSS/TM/ETM+/OLI archive: 42 years of our history. Analysis of Multitemporal Remote Sensing Images (MultiTemp), 2017 9th International Workshop on the. pp. 1–9.
Schuler, M., Stucki, E., Roque, O., Perlik, M., 2004. Mountain Areas in Europe: Analysis of Mountain Areas in EU Member States, Acceding and Other European Countries.
Selkowitz, D.J., Forster, R.R., 2015. An automated approach for mapping persistent ice and snow cover over high latitude regions. Remote Sens. 8, 16.
Severskiy, I.V., Zichu, X., 2000. Snow Cover and Avalanches in the Tien Shan Mountains. Minist. Educ. Sci. Repub. Kazakhstan, Acad. Sci. China. Almaty, VAC, pp. 310.
Tachikawa, T., Hato, M., Kaku, M., Iwasaki, A., 2011. Characteristics of ASTER GDEM version 2. Geoscience and Remote Sensing Symposium (IGARSS), 2011 IEEE International. pp. 3657–3660.
USGS/EROS, 2017. Landsat Collection 1 Level 1 Product Definition - Version 1. Sioux Falls, SD, USA (accessed 19 July 2018). https://landsat.usgs.gov/sites/default/files/documents/LSDS-1656_Landsat_Level-1_Product_Collection_Definition.pdf.
Wayand, N.E., Marsh, C.B., Shea, J.M., Pomeroy, J.W., 2018. Globally scalable alpine snow metrics. Remote Sens. Environ. 213, 61–72.
WMO, 2007. The Role of Climatological Normals in a Changing Climate. World Meteorol. Organ (accessed 19 July 2018). https://library.wmo.int/doc_num.php?explnum_id=4546.
Wulder, M.A., Masek, J.G., Cohen, W.B., Loveland, T.R., Woodcock, C.E., 2012. Opening the archive: how free data has enabled the science and monitoring promise of Landsat. Remote Sens. Environ. 122, 2–10.
Wulder, M.A., White, J.C., Loveland, T.R., Woodcock, C.E., Belward, A.S., Cohen, W.B., Fosnight, E.A., Shaw, J., Masek, J.G., Roy, D.P., 2016. The global Landsat archive: status, consolidation, and direction. Remote Sens. Environ. 185, 271–283.
Zhu, Z., Woodcock, C.E., 2012. Object-based cloud and cloud shadow detection in Landsat imagery. Remote Sens. Environ. 118, 83–94.
Zhu, Z., Wang, S., Woodcock, C.E., 2015. Improvement and expansion of the Fmask algorithm: Cloud, cloud shadow, and snow detection for Landsats 4–7, 8, and Sentinel 2 images. Remote Sens. Environ. 159, 269–277.